Dalton Transactions

Accepted Manuscript

ROYAL SOCIETY OF CHEMISTRY

www.rsc.org/dalton

Table of contents entry.

Plasmoic Ag nanocrystals were in-situ decorated on 3D $(BiO)_2CO_3$ hierarchical microspheres for enhanced visible light photocatalysis and photocurrent generation by an one-pot in situ hydrothermal method.

TOC Graphic

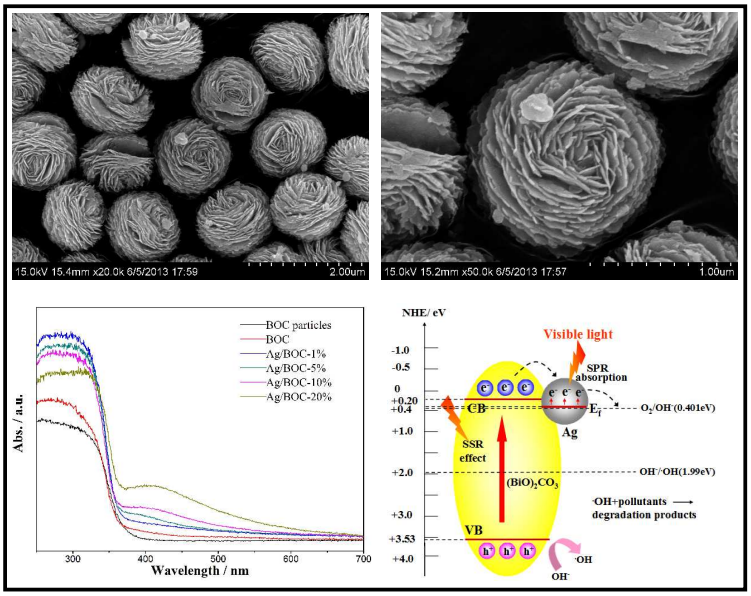

Journal Name

Dynamic Article Links ►

Cite this: DOI: 10.1039/c0xx00000x

www.rsc.org/xxxxxx

ARTICLE TYPE

In situ decoration of plasmonic Ag nanocrystals on the surface of $(BiO)_2CO_3$ hierarchical microspheres for enhanced visible light photocatalysis

Fan Dong [a,*], Qiuyan Li [a], Ying Zhou [b], Yanjun Sun [a], Haidong Zhang [a], Zhongbiao Wu [c]

Received (in XXX, XXX) Xth XXXXXXXXX 20XX, Accepted Xth XXXXXXXXX 20XX
DOI: 10.1039/b000000x

Abstract: Novel plasmonic 0D Ag nanocrystal decorated 3D $(BiO)_2CO_3$ hierarchical microspheres were fabricated with a one-pot hydrothermal method. The as-prepared samples were systematically characterized by X-ray diffraction, scanning electron microscopy, transmission electron microscopy, N_2 adsorption-desorption isotherms, X-ray photoelectron spectroscopy, UV-vis diffuse reflectance spectroscopy, photoluminescence spectra, ns-level time-resolved fluorescence spectra, photocurrent generation and EIS measurement. The results indicated that the 0D Ag nanoparticles were deposited on the surface of 3D $(BiO)_2CO_3$ hierarchical microspheres. The deposited Ag nanoparticles were reduced from Ag^+ by citrate ions from bismuth citrate. The photocatalytic activity of the as-prepared samples was evaluated towards degradation of NO at ppb-level under visible light irradiation. The intermediate of NO_2 during photocatalytic reaction was monitored on-line. The pure $(BiO)_2CO_3$ microspheres exhibited decent visible light photocatalytic activity because of the surface scattering and reflecting (SSR effect) resulting from the special 3D hierarchical architecture. The Ag-decorated $(BiO)_2CO_3$ microspheres (Ag/BOC) exhibited greatly enhanced photocatalytic activity, photocurrent generation and promoted NO_2 oxidation compared to pure $(BiO)_2CO_3$ microspheres. The enhanced photocatalytic activity and photocurrent generation of Ag/BOC was ascribed to the cooperative contribution of the surface plasmon resonance (SPR effect), efficient separation of electron-hole pairs and prolonged lifetime of charge carriers induced by Ag nanoparticles. The photocatalytic performance of Ag/BOC was dependent on the contents of Ag loading. When the amount of Ag was controlled at 5%, the highest photocatalytic performance can be achieved. Further increasing the Ag loading content could promote the aggregation of Ag particles and transform the uniform microspheres into un-uniform microspheres, which is not beneficial to improve the activity. Importantly, the as-prepared Ag/BOC composites exhibited high photochemical stability after multiple reaction runs. The concepts of enhancing the activity through the SSR and SPR effects provide a new avenue for the development of efficient noble metal/bismuth-based plasmonic photocatalysts with attractive nano/micro architectures for efficient visible light photocatalytic activity.

Keywords: Ag-decorated $(BiO)_2CO_3$; Hydrothermal synthesis; Surface plasmon resonance; surface scattering and reflecting; Visible light photocatalysis; Charge separation.

∗ To whom correspondence should be addressed. E-mail: dfctbu@126.com
Tel.: +86-23-62769785-605; Fax: +86-23-62769785-605
[a] Chongqing Key Laboratory of Catalysis and Functional Organic Molecules, College of Environmental and Biological Engineering, Chongqing Technology and Business University, Chongqing, 400067, China.
[b] State Key Laboratory of Oil and Gas Reservoir and Exploitation, School of Materials Science and Engineering, Southwest Petroleum University, Chengdu, 610500, China
[c] Department of Environmental Engineering, Zhejiang University, Hangzhou, 310027, China.

1. Introduction

Photocatalysis is a highly appealing technology with multiple applications, mainly in the fields of pollution control, solar fuel production and chemical synthesis. In the past few decades, many semiconductor photocatalytic materials have been synthesized, including UV-excited and visible-excited semiconductors.[1-3] It's well known that the application of traditional UV-responsive photocatalysts is limited by its large band gap, which cannot use the solar energy effectively. Therefore, the development of visible light (46% fraction of solar light) responsive photocatalysts with narrow band gap is urgent and highly desirable, which could provide a potential route for environmental pollution and clean energy development.[1-3] Various approaches have been employed to improve the visible light activity of photocatalysts, such as metal doping, nonmetal doping, composites and noble-metal deposition, sensitization and so on.[4-6]

Recently, the noble-metal based plasmonic photocatalyst working under visible light has attracted great attention. The plasmonic photocatalyst consisted of noble metal and semiconductor possesses a significant effect of surface plasmon resonance (SPR) that enables the photocatalyst to absorb visible light. The SPR effect can be described as the resonant photon-induced collective oscillation of valence electrons established when the frequency of photons matches the natural frequency of surface electrons oscillating against the restoring force of positive nuclei.[7-9] To date, some plasmonic photocatalysts have been reported, such as Ag@AgX (X=Cl, Br),[10-11] M@TiO_2 (M=Au, Pt, Ag),[12] Pt/Bi_2O_3,[13] Ag/AgCl/TiO_2[14] and Ag-AgI/Fe_3O_4@SiO_2.[15] All these plasmonic photocacalysts exhibited an enhanced photocatalytic activity comparing with the substrate semiconductors.

$(BiO)_2CO_3$ is a new multifunctional material and has received great research interests recent years.[16-27] For example, Chen and co-workers have prepared $(BiO)_2CO_3$ nanotubes with antibacterial performance.[16] They also hydrothermally synthesized $(BiO)_2CO_3$ nanobars, nanoplates and cube-like.[17] Xie's group have synthesized various $(BiO)_2CO_3$ microstructures to degrade aqueous dye Rhodamine B (RhB).[18] $(BiO)_2CO_3$ nanosheets and flower-like structures were prepared by Huang *et al*.[19] Cao's group have fabricated persimmon-like $(BiO)_2CO_3$, which was able to efficiently degrade RhB and eosin sodium salt under simulated solar light irradiation.[20] Zhang et al reported morphogenesis and self-assembly of 3D $(BiO)_2CO_3$ hierarchical nanostructures for ultrasensitive detection of aromatic molecules.[21] However, $(BiO)_2CO_3$ nanoparticles with a big band gap (3.1~3.5 eV) can only be excited by UV light. In order to improve the activity of $(BiO)_2CO_3$ under visible light irradiation, Yu and co-workers have reported $BiVO_4$/$(BiO)_2CO_3$ and graphene/$(BiO)_2CO_3$ nanocomposites which exhibited enhanced visible light photocatalytic activity.[22-23] Dong's group have fabricated N-doped $(BiO)_2CO_3$ hierarchical microspheres with outstanding photocatalytic activity under visible light irradiation.[24-26] Peng at al prepared $Bi_2O_2CO_3$ nanoplates microspheres by VPV-assisted hydrothermal method.[27] Ag is then deposited on the surface of $Bi_2O_2CO_3$ via a subsequent photoreduction process for enhanced photocatalytic activity and supercapacitor performance.[27] Although, semiconductor compositing and N-doping could make the pure $(BiO)_2CO_3$ visible light active, there is little report on the noble metal/$(BiO)_2CO_3$-based plasmonic photocatalysts with 3D hierarchical structures. On one hand, the 3D hierarchical structures could make the pure $(BiO)_2CO_3$ visible light active through surface scattering and reflecting effects (SSR effect). On the other hand, noble metal decoration could further enhance the visible light activity of 3D $(BiO)_2CO_3$ hierarchical microspheres through surface plasmon resonance effects (SPR effect).

In the present study, we developed a one-pot hydrothermal method to in-situ deposit plasmonic Ag nanocrystal on $(BiO)_2CO_3$ hierarchical microspheres in order to promote the visible light photocatalytic activity of $(BiO)_2CO_3$ microspheres. In the hydrothermal process, Ag^+ was reduced to metal Ag by citrate ions from bismuth citrate. The pure $(BiO)_2CO_3$ microspheres exhibited decent visible light activity because of the surface scattering and reflecting effects induced by the 3D hierarchical structures. The novel Ag-decorated $(BiO)_2CO_3$ microspheres composites exhibited dramatically enhanced photocatalytic activity towards NO degradation compared with pure $(BiO)_2CO_3$ microspheres because of the cooperative contribution of the SPR effect, efficient separation of electron-hole pairs and prolonged lifetime of charge carriers by Ag nanoparticles. Meanwhile, the effect of Ag content on the photocatalytic performance was evaluated. The sample with 5% Ag loading exhibited the highest photocatalytic activity. More importantly, the excellent photocatalyst showed high photochemical stability and durability, which is significant for its practical application. By combination of the SSR effect and SPR effect, efficient and durable visible light driven photocatalyst can be developed, which could provide new insights into the design and synthesis of novel photocatalytic materials for environmental and energetic applications.

2. Experimental section

2.1 Synthesis of Ag-decorated $(BiO)_2CO_3$ samples

All the chemicals employed in this study were analytical grade and were used without further purification. Distilled water was used in all experiments. In a typical synthesis process, sodium carbonate (0.46 g) was first dissolved in distilled water (70 ml) in a 100 ml autoclave Teflon vessel and stirred for 10 min. Then 0.04 mol/L $AgNO_3$ solution with appropriate volume was added into the solution and further stirred for 10 min. Afterwards, bismuth citrate (1.6g) was added into the above solution and the mixture was stirred for 30 min to ensure that all reagents dissolved sufficiently. The resulting precursor suspension was hydrothermally treated at 160 ^oC for 24h. After being cooled down to room temperature, the resulting solid was filtered, washed with water and ethanol four times and dried at 60 ^oC for 12h to get final Ag-decorated

$(BiO)_2CO_3$ sample. In order to investigate the effects of Ag content on the photocatalytic activity of Ag-decorated $(BiO)_2CO_3$, the amount of $AgNO_3$ solution was controlled at 0.5, 2.5, 5.0 and 10.0 ml, the obtained samples were labeled as Ag/BOC-1%, Ag/BOC-5%, Ag/BOC-10% and Ag/BOC-20%, respectively. Pure $(BiO)_2CO_3$ microspheres (labeled as BOC) a were prepared as references without adding $AgNO_3$. As a reference, $(BiO)_2CO_3$ with nanosheet morphology (labelled as BOC nanosheet) was prepared (Fig. S1).[25]

2.2 Characterization

The X-ray diffraction patterns of the samples were collected on an X-ray diffractometer with Cu Kα radiation (XRD: model D/max RA, Rigaku Co., Japan). In order to characterize the morphology, structure and grain size of the obtained products, scanning electron microscope (SEM: JEOL model JSM-6490, Japan), transmission electron microscope (TEM: JEM-2010, Japan, and high-resolution transmission electron microscope (HRTEM, were used to collect the SEM and TEM images. The Brunauer–Emmett–Teller (BET) specific surface area (S_{BET}) and pore structure of the samples were analyzed by Nitrogen adsorption-desorption in a nitrogen adsorption apparatus (ASAP 2020, USA, with all samples degassed at 100°C for 12 h prior to measurements. X-ray photoelectron spectroscopy measurement was carried out to investigate the surface chemical compositions and its chemical state, using Al Kα X-rays ($h\nu$ = 1486.6 eV) radiation source operated at 150 W (XPS: Thermo ESCALAB 250, USA). The UV-vis diffuse reflection spectra were obtained for the dry-pressed disk samples with a Scan UV-vis spectrophotometer (UV-vis DRS: UV-2450, Shimadzu, Japan), using $BaSO_4$ as a standard sample. The Photoluminescence (PL: F-7000, HITACHI, Japan, was used to investigate the optical properties of the obtained samples. Steady and time-resolved fluorescence emission spectra were recorded at room temperature with a fluorescence spectrophotometer (Edinburgh Instruments, FLSP-920).

2.3 Evaluation of photocatalytic activity

The photocatalytic activity of the as-synthesized samples was evaluated by removing NO at ppb level in a continuous flow reactor (Fig. S2 shows the photo of the reactor system). The volume of the reactor was 4.5 L (30 cm × 15 cm × 10 cm), made of polymeric glass and covered with Saint-Glass. There was a commercial tungsten halogen lamp (150 W, vertically placed 20 cm above the reactor. UV cutoff filter (420 nm) was applied to remove UV light for the test of visible light photocatalytic activity. The as-prepared sample (0.20g) was dispersed in distilled water (50 ml) in a beaker by ultrasonic treatment for 10 min, and then coated onto two glass dishes with a diameter of 12.0 cm. The coated dishes were pretreated at 70°C to remove water in the suspension and placed in the center of the reactor after cooling down to room temperature. The NO gas was acquired from a compressed gas cylinder at a concentration of 100 ppm of NO (N_2 balance). The initial concentration of NO was diluted to about 600 ppb by the air stream. The flow rate of air stream and NO were controlled at 2.4 L min^{-1} and 15 mL min^{-1}, respectively. Then the two gas streams were premixed by a three-way valve. After the adsorption-desorption equilibrium was achieved, the lamp was turned on. The concentration of NO was measured by a NO_x analyzer (Thermo Scientific, 42i-TL) every one min, which also monitors the concentration of NO_2 and NO_x (NO_x represents NO + NO_2). The removal ratio of NO (η) was calculated by η (%) = $(1 - C/C_0) \times 100\%$, C is the outlet concentration of NO after reaction for time t and C_0 represents the inlet concentration after achieving adsorption-desorption equilibrium.

3. Results and discussion

3.1 Phase structure

XRD was used to characterize the phase structure of the as-prepared samples. Fig. 1 shows the XRD patterns of the products with different Ag content. It can be seen that all the samples are well crystallized. The diffraction peaks of BOC without adding $AgNO_3$ can be readily indexed to the tetragonal $(BiO)_2CO_3$ structure (JCPDS-ICDD Card No. 41-1488) and no other impurities are detected, indicating a pure $(BiO)_2CO_3$ phase. When $AgNO_3$ was used as a precursor in the fabrication of samples, new diffraction peaks at 2θ = 38° and 44° are observed in Ag/BOC-5%, Ag/BOC-10% and Ag/BOC-20% in addition to the characteristic peaks of pure $(BiO)_2CO_3$ phase. These new peaks are ascribed to the deposition of Ag nanoparticles (JCPDS-ICDD Card No. 65-2871) on the surface of $(BiO)_2CO_3$ microspheres. However, such new peaks are not detected in Ag/BOC-1% sample for its low amount of Ag. The formation of Ag nanoparticles derived from the reduction of Ag^+ by citrate ions in bismuth citrate. Based on further observation, the peak intensity of Ag nanoparticles is increased gradually with the increasing Ag content, while some diffraction peaks of $(BiO)_2CO_3$ in Ag/BOC-20% are decreased, suggesting that high Ag content would affect the crystallinity of $(BiO)_2CO_3$. Meanwhile, it's noteworthy to mention that the changes of all diffraction peaks and lattice parameters of $(BiO)_2CO_3$ in Ag/BOC samples are not detectable, which implies that Ag did not get into the lattice of $(BiO)_2CO_3$, but on the surface.[25,26] According to the crystal structure of $(BiO)_2CO_3$, the $(Bi_2O_2)^{2+}$ layers and CO_3^{2-} layers are orthogonally inter-grown. The internal layered structure would mediate lower growth rate along certain axis to form nanosheet morphology.[24,28]

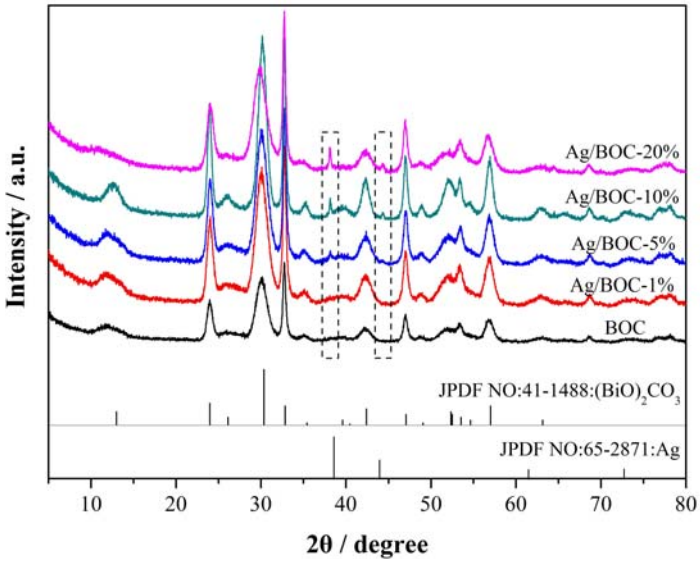

Fig. 1 XRD patterns of the samples obtained in the presence of different amount of Ag.

3.2 Morphological structure

The morphology and microstructure of the obtained samples were characterized by SEM, TEM and HRTEM. In Fig. 2a and 2b, we can easily find that the pure $(BiO)_2CO_3$ sample consists of many three-dimensional (3D) flower-like hierarchical microspheres self-assembled by two-dimensional (2D) nanosheets. Obviously, these microspheres are in different sizes from 0.7 to 1.3μm. Compared with the pure $(BiO)_2CO_3$ microspheres, the Ag/BOC-1% microspheres are more uniform due to the addition of $AgNO_3$ (2c, 2d). The Ag nanoparticles cannot be observed on the surface of $(BiO)_2CO_3$ microspheres due to its low loading content. This result is in agreement with the XRD observation.

SEM, TEM, HRTEM and SAED images of Ag/BOC-5% sample are shown in Fig. 3. The SEM images in Fig. 3a and 3b show that these microspheres become uniform as the amount of Ag is increased from 1% to 5%. Some zero-dimensional (0D) monodispersed Ag nanoparticles (circled by dotted line) are deposited on the surface of 3D uniform $(BiO)_2CO_3$ microspheres with an average diameter of about 1.5μm. The corresponding EDS spectra (Fig. 3c and 3d) confirm the amount of Ag at the particle is 8 %, while no Ag is detected beside the particle, indicating that Ag was deposited on the surface of the microspheres instead of doping into it. It's presumed that the formation of Ag nanoparticles derived from the reduction of Ag^+ by citrate ions in bismuth citrate. Such special microstructures consisted of 0D nanoparticles and 3D flower-like hierarchical microspheres have never been reported before. The morphological structures of the sample were further confirmed by TEM and HRTEM. As shown in Fig. 3e and 3f, the microspheres are indeed composed of self-assembled nanosheets with monodispersed Ag nanoparticles attaching on the surface (circled by dotted line). Fig. 3g shows the typical HRTEM image of Ag/BOC-5%, the lattice spacing is determined to be 0.254nm and 0.235nm, which correspond to the (112) crystal plane of tetragonal $(BiO)_2CO_3$ and (111) lattice plane of Ag, respectively. The SAED image (Fig. 3h) of one single nanosheet reveals two different kinds of diffraction spots that can be indexed to tetragonal $(BiO)_2CO_3$ and Ag, respectively. The regular diffraction spots also indicate that the nanosheet is single-crystalline in nature.

Fig. 4 shows the SEM images of Ag/BOC-10%. Obviously, more Ag nanoparticles are formed on the surface of 3D $(BiO)_2CO_3$ microspheres compared to Ag/BOC-5% and few particles begin to aggregate. In addition, for part of the microspheres, the nanosheets assembled more compact and with a diameter of about 200 nm. When the amount of $AgNO_3$ was increased to 10.0 ml, all the flower-like hierarchical microspheres are transformed into un-uniform hierarchical microspheres (Fig. S3a). The high-magnification SEM image (Fig. S3b) reveals that Ag nanoparticles are aggregated together on the surface of $(BiO)_2CO_3$ microspheres. The gradually increased Ag aggregations on the surface of $(BiO)_2CO_3$ microspheres corresponds to the gradually increased peak intensity in the XRD pattern. Consequently, the amount of $AgNO_3$ plays a cardinal role in the formation of the as-prepared samples and then affects its photocatalytic activity.

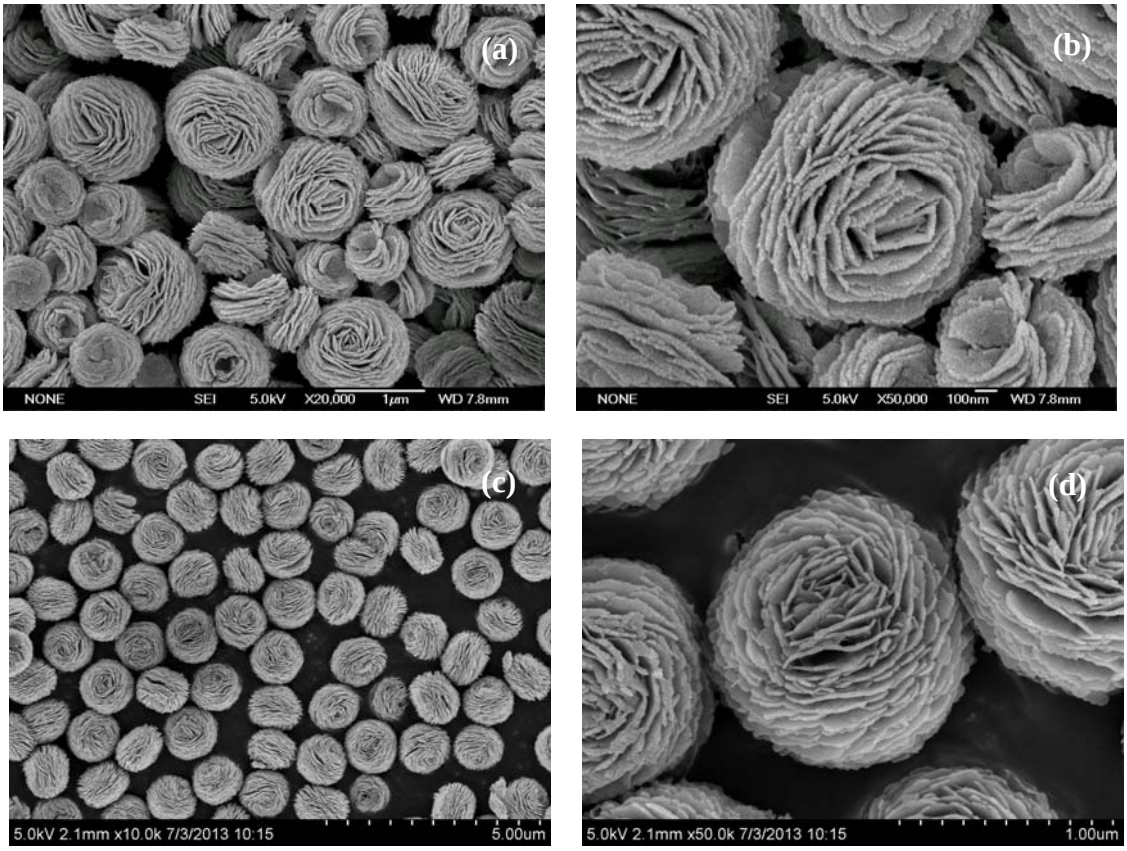

Fig. 2 SEM images of BOC (a, b) and Ag/BOC-1% (c, d)

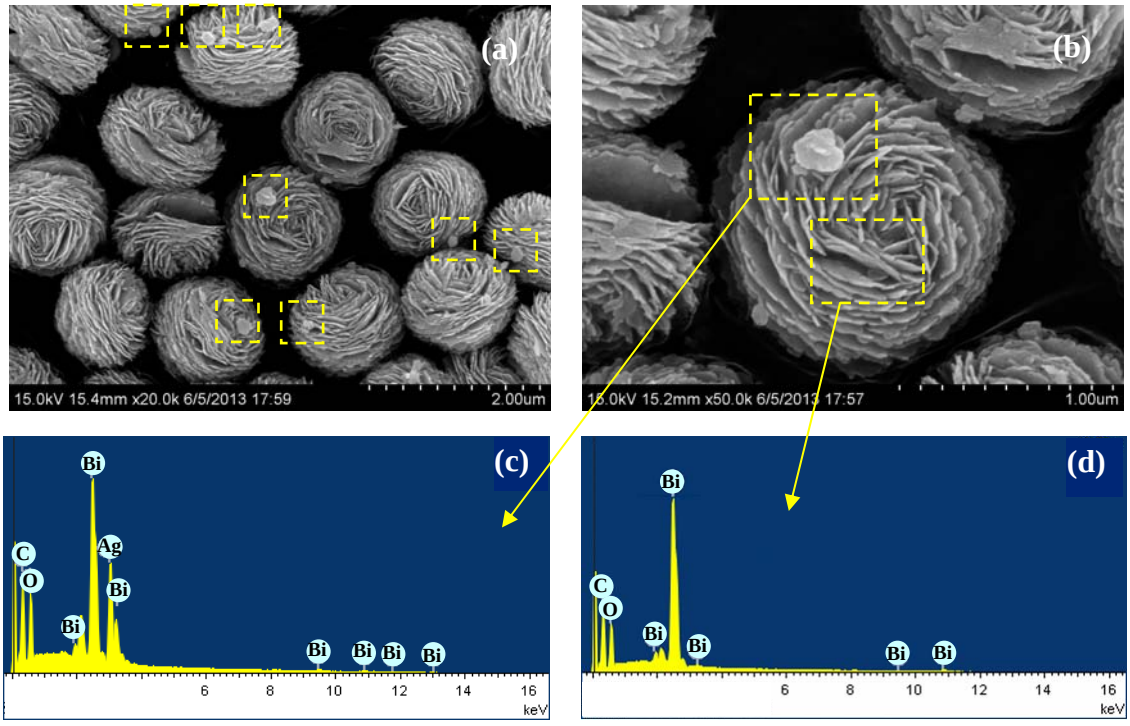

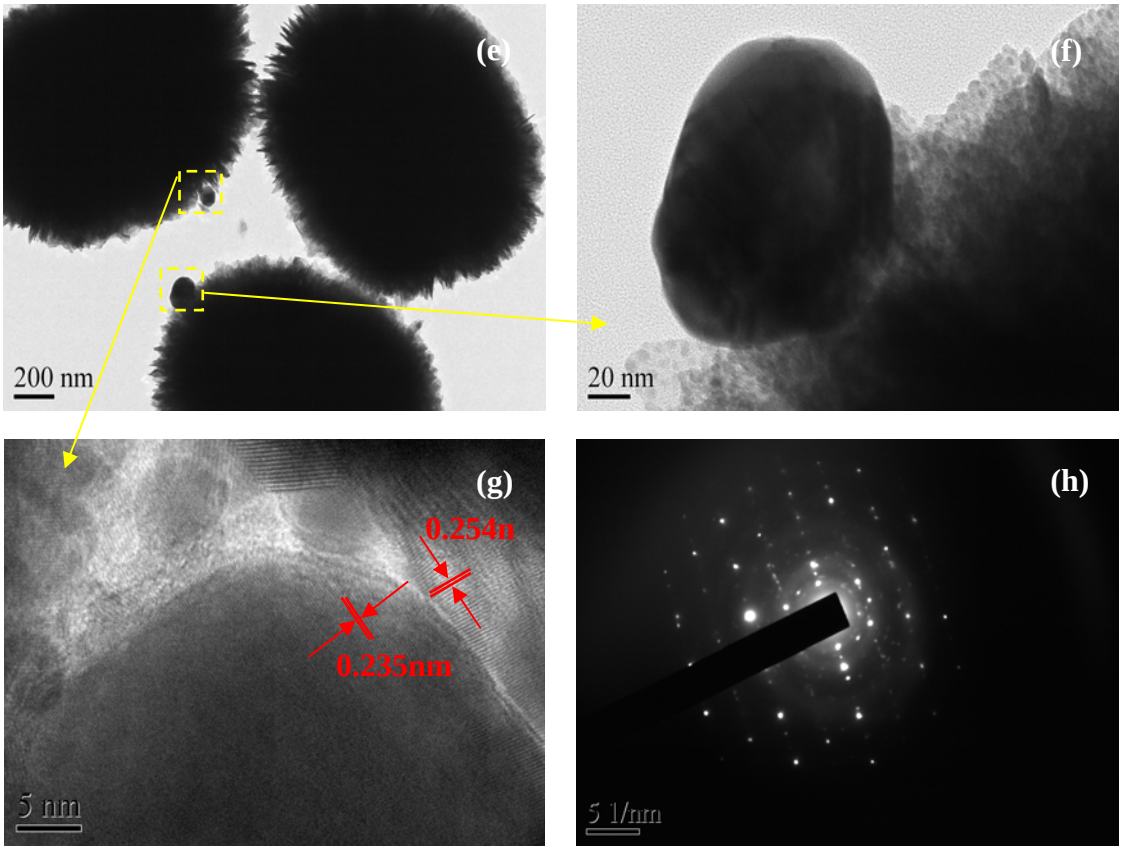

Fig. 3 SEM (a, b), EDS (c, d), TEM (e, f), HRTEM (g) and SAED (h) images of Ag/BOC-5%.

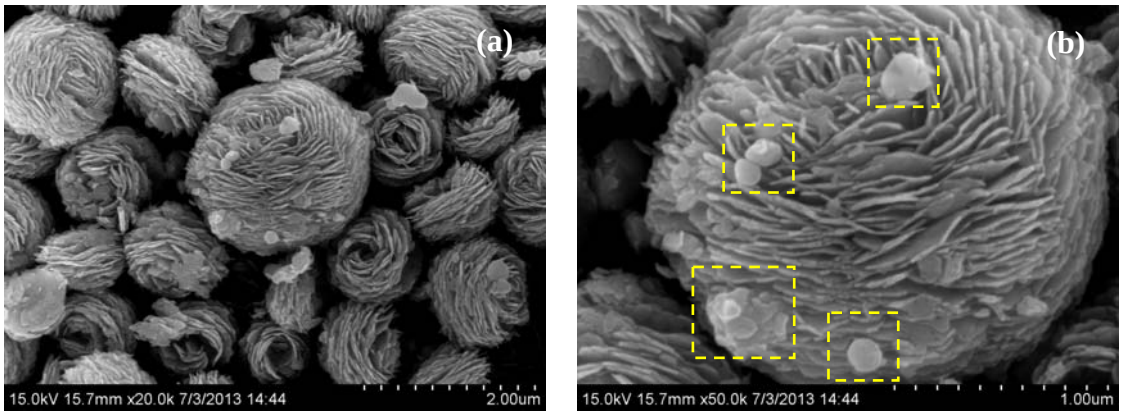

Fig. 4 SEM images of Ag/BOC-10%.

3.3 BET surface areas and pore structure

The nitrogen adsorption-desorption isotherms and corresponding pore size distribution curves of the as-prepared samples are displayed in Fig. 5. According to the Brunauer-Deming-Deming-Teller (BDDT) classification, the majority of physisorption isotherms can be classified into six types. Typically, the Ag/BOC-5% and pure BOC both have an isotherm of type IV, indicating the presence of mesopores (Fig. 5a). The Ag/BOC-5% displays a higher absorption at the relatively high pressure comparing with BOC, suggesting the presence of more large mesopores in Ag/BOC-5%. This result is also demonstrated by the pore-size distribution curves. The increased large mesopores are probably caused by the addition of $AgNO_3$ that changes the morphologies of the samples. Furthermore, the shape of the hysteresis loops is of type H3, implying the existence of slit-like pores.[29-30] The result is consistent with the SEM observations. The corresponding pore size distribution curves of the samples are shown in Fig. 5b. It can be seen that the pore-size distribution range for the

samples is broad in the range of 2 to 80 nm and bimodal with small mesopores (3 nm) and larger ones (10 nm), confirming the formation of mesopores.[31-32] The small mesopores can be attributed to the pores formed among the aggregated nanosheets and the large mesopores are ascribed to the pores formed between the microspheres. The BET surface areas of BOC, Ag/BOC-1%, Ag/BOC-5%, Ag/BOC-10% and Ag/BOC-20% are measured to be 46, 45, 44, 41 and 37 m^2/g, indicating that the surface decoration of Ag nanocrystals exerts little impact on the BET surface areas of BOC. In general, the porous structures are expected to be useful in the photocatalytic process by offering efficient transport pathways for reactants and the products and facilitating the adsorption of pollutants for degradation.[33]

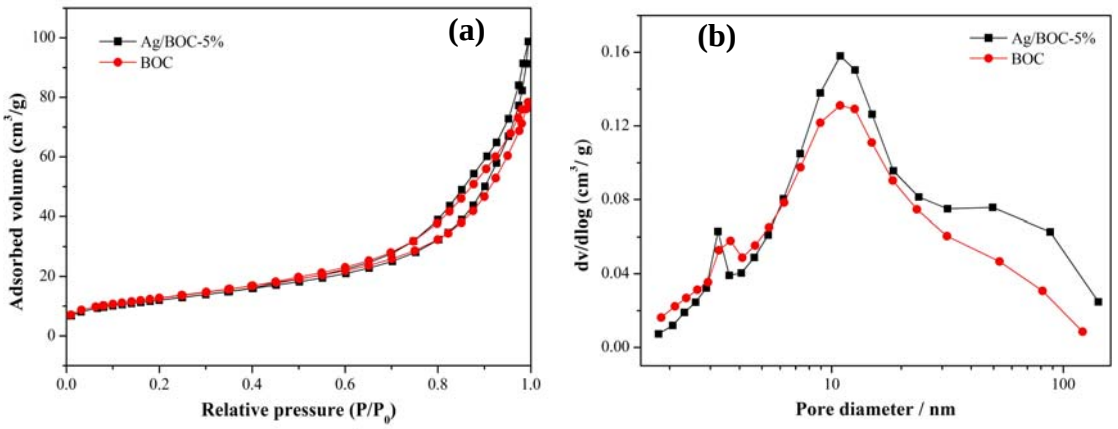

Fig. 5 N_2 adsorption-desorption isotherms (a) and pore size-distribution curves (b) of Ag/BOC-5% and BOC.

3.4 Chemical composition by XPS

The XPS measurement was carried out to elucidate the chemical state of the elements on the surface of Ag/BOC-10% sample, as shown in Fig. 6. The two strong peaks at 159.1 and 164.4 eV in the spectra (Fig. 6a) are assigned to $Bi4f_{7/2}$ and $Bi4f_{5/2}$, respectively, which is the feature of Bi^{3+} in $(BiO)_2CO_3$.[34] Fig. 6b shows the C1s spectra of $(BiO)_2CO_3$. The peak at 284.78 eV is caused by the adventitious carbon species, while the peak at 288.7 eV can be ascribed to the CO_3^{-2} in $(BiO)_2CO_3$. The O1s peak (Fig. 6c) at 530.99 is characteristic of Bi-O in $(BiO)_2CO_3$. The spectra of $Ag3d_{3/2}$ and $Ag3d_{5/2}$ (Fig. 6d) were recorded, which are identified at 374.1 and 368.2 eV, indicating that Ag^+ was reduced to metal Ag by citrate ion in bismuth citrate.[35] The result also has been demonstrated by XRD and SEM analysis.

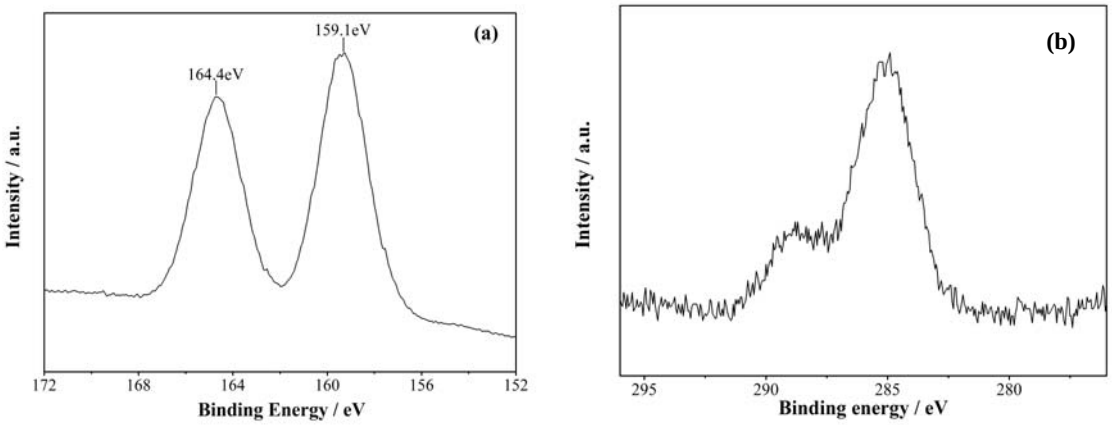

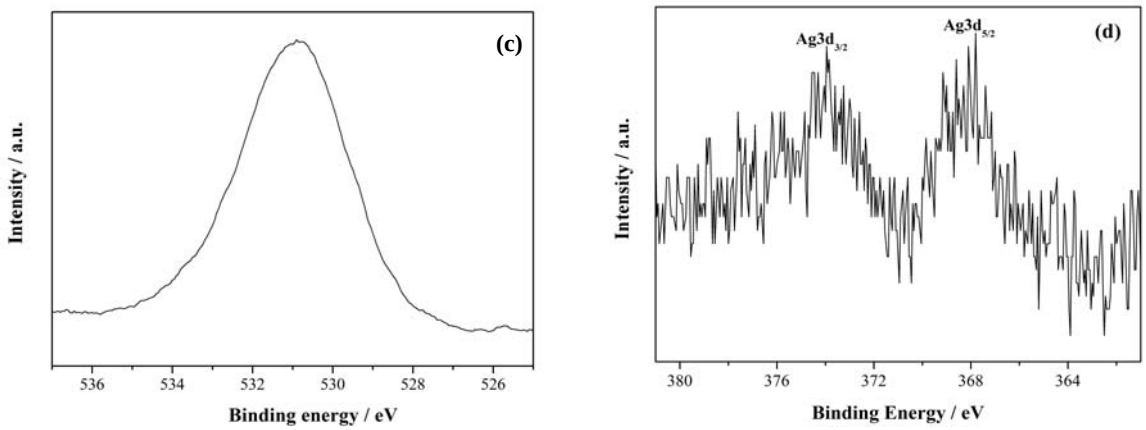

Fig. 6 XPS spectra of Ag/BOC-5%, Bi4f (a), C1s (b), O1s (c), Ag3d (d).

3.5 Light absorption, charge separation and carriers lifetime

It's well known that the optical properties of the semiconductors are closely related to its photocatalytic activity. The UV-vis DRS spectra of Ag/BOC and pure $(BiO)_2CO_3$ samples are shown in Fig. 7. In the UV region, all the samples in the presence of Ag display higher absorption compared with pure $(BiO)_2CO_3$, probably due to the addition of $AgNO_3$. In addition, the $(BiO)_2CO_3$ microspheres exhibit higher absorption than $(BiO)_2CO_3$ nanosheets both in the UV and visible light region, which is relevant to its special 3D hierarchical structure (SEM Fig. 2). This special hierarchical structure could generate multiple light scattering and reflecting effects, thus greatly increasing effective optical path-length of a photon and absorption probability.[40] It's noteworthy to mention that there is a broad absorption in the visible light region from 400 nm to 600 nm for Ag/BOC-5%, Ag/BOC-10% and Ag/BOC-20%, centered at 415 nm. Such absorption ability in the visible light region should be attributed to the SPR effect of spatially confined electrons in metallic Ag nanoparticles.[36-37] Previous report has demonstrated that Ag nanoparticles with 100 nm diameter could exhibit a SPR absorption centered at 415 nm.[38] However, the Ag/BOC-1% sample does not exhibit such phenomenon due to the low content of Ag. The above results are in agreement with the XRD and SEM analysis. The samples exhibit increased absorption in the visible light region with increasing Ag content. This can be ascribed to the stronger SPR effect caused by more deposited Ag nanoparticles, therefore absorbing more solar light.[36-37] In general, the special 3D hierarchical structure could make $(BiO)_2CO_3$ absorbe certain visible light through the light reflecting and scattering. And the deposition of Ag nanoparticles on the surface of $(BiO)_2CO_3$ microspheres could further significantly enhance the visible light absorption.

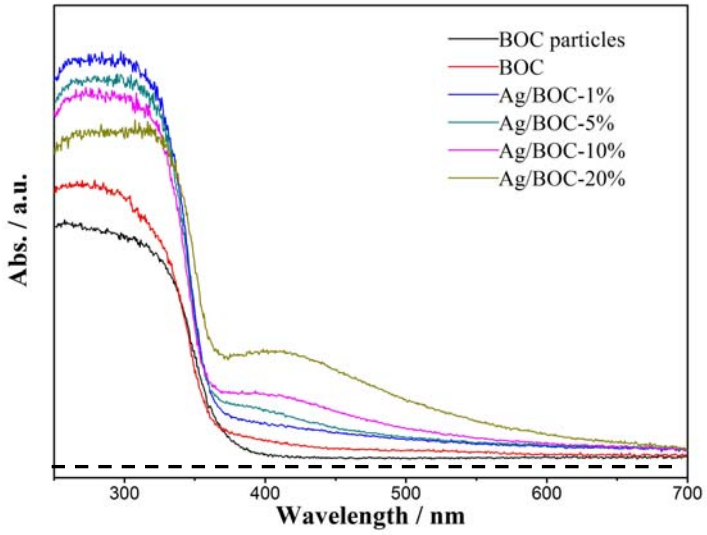

Fig. 7 UV-vis DRS spectra of the samples with different amount of Ag and pure $(BiO)_2CO_3$.

The recombination of electron-hole pairs was measured by PL. Fig. 8 shows the PL spectra of Ag/BOC and pure $(BiO)_2CO_3$ samples with an excitation wavelength of 280 nm. It can be seen that the fluorescence emission peaks are mainly centered at 325-500 nm, which contains both UV and visible light region. This result reveals that the as-prepared samples are able to absorb both UV and visible light. The absorption for visible light can be ascribed to the special hierarchical structures of $(BiO)_2CO_3$ microspheres and SPR effect of Ag nanoparticles, which have been demonstrated by

UV-vis DRS analysis. Furthermore, the peak intensity of BOC is stronger than that of all the Ag/BOC samples, suggesting that the recombination rate of electron-hole pairs on Ag/BOC samples is lower than BOC. This result is supported by the fact that the deposited Ag nanoparticles can act as electron traps adding electron-hole separation.[39-40] Meanwhile, the peak intensity decreased with the increasing Ag content, which suggests that more Ag nanoparticles can trap more electrons and reduce electron-hole recombination. In a word, the presence of metal Ag nanoparticles will play a crucial role in separating the electron-hole pairs.

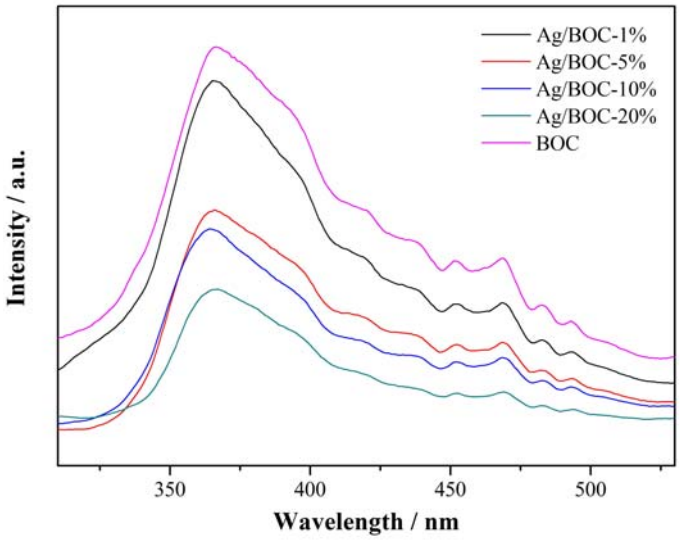

Fig. 8 PL spectra of the Ag/BOC samples with different amount of Ag and pure $(BiO)_2CO_3$.

To investigate the photophysical property of photoexcited charge carriers of BOC and Ag/BOC-5%, the ns-level time-resolved fluorescence decay spectra were recorded, as shown in Fig. 9a and 9b. The radiative lifetime with different percentages can be determined by fitting the decay spectra, as summarized in Table 1. The short lifetime (τ_1) of BOC is 0.35 ns. After Ag decoration, the short lifetime of Ag/BOC-5% is increased up to 0.54 ns. The percentage of charge carriers with short lifetime of the two samples shows little change. The long lifetime (τ_2) of charge carriers is increased from 4.25 ns for BOC to 5.54 ns for Ag/BOC-5%. The percentage of charge carriers with long lifetime is also increased slightly after Ag decoration. These results imply that the radiative lifetime of all charge carriers are increased by formation of Ag/BOC composites. The photoexcited electrons transfer from $(BiO)_2CO_3$ to Ag nanoparticles are responsible for the prolonged lifetime of charge carriers. The prolonged lifetime of charge carriers could increase its probability of being captured by reactive substrates to initiate the following photocatalytic reactions.

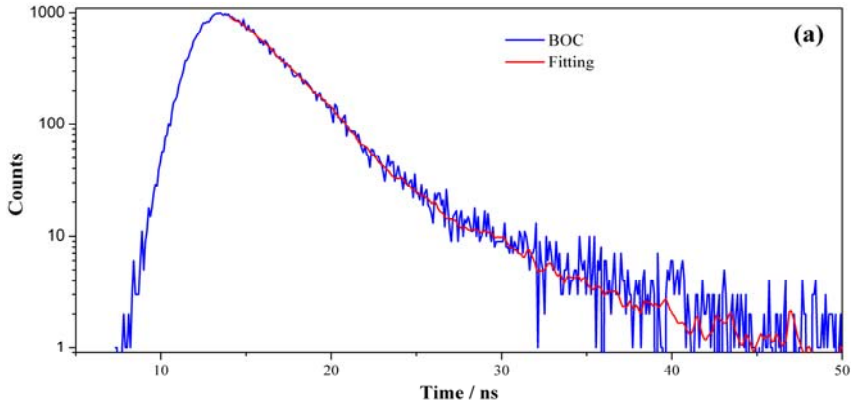

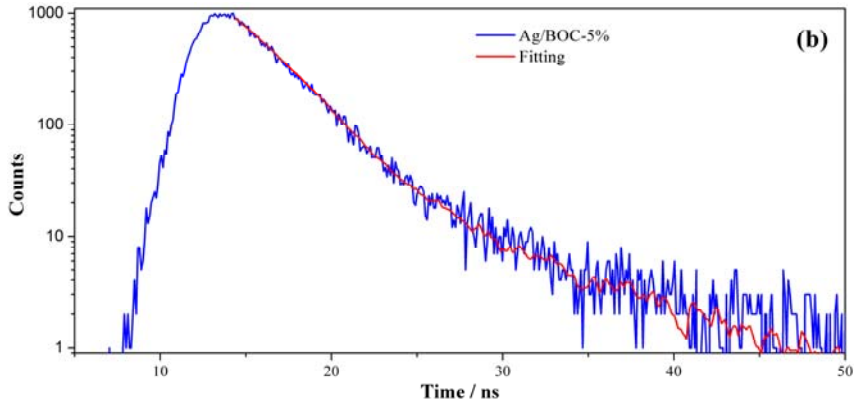

Fig. 9 The ns-level time-resolved fluorescence spectra monitored at 440 nm under 375 nm excitation at room temperature for BOC (a) and Ag/BOC-5% (b) samples.

Table 1 The kinetics of emission decay parameters of BOC and Ag/BOC-5% samples.[a]

Samples	Component	Life time (ns)	Relative Percentage (%)	χ^2
BOC	τ_1	0.35	95.57	1.021
	τ_2	4.25	4.43	
Ag/BOC-5%	τ_1	0.54	95.38	1.062
	τ_2	5.54	4.62	

[a] The decay spectra were fitted by the equation $f(t)=A+\sum_{i=1}^{N} B_i e^{-t/\tau_i}$.

3.6 Photocatalytic activity and photocurrent generation

NO with concentration at ppb level is a representative indoor and outdoor air pollutant. The obtained Ag/BOC samples were employed to photocatalytic removal of NO in air to demonstrate their potential ability for air pollutant degradation. As previous reported, NO was very stable and cannot be photolyzed under light irradiation without photocatalysts.[34] However, in the presence of photocatalytic materials, NO reacted with the photogenerated reactive radicals to produce NO_2 intermediate and transform to final HNO_3 product.[25,34]

Fig. 10a shows the variation of NO concentration (C/C_0%) with irradiation time over Ag/BOC samples under visible light irradiation with pure $(BiO)_2CO_3$ as references. The pure $(BiO)_2CO_3$ with nanosheet morphology (see Fig. S1) shows little activity under visible light irradiation. However, a decent removal ratio of 22% is observed on pure $(BiO)_2CO_3$ with microspheres morphology (see Fig. 2a) under the same conditions. This fact could be ascribed to the special hierarchical structures in $(BiO)_2CO_3$ microspheres (SEM in Fig. 2), which could induce the effects of multiple light surface scattering and reflecting (SSR effect), thus greatly increasing effective optical path-length of a photon and absorption probability (Fig. 7).[41] Similar phenomenon has been observed on BiOCl hierarchical nanostructures.[41] From BET analysis, the hierarchical structures can also offer efficient transport pathways for reactants and products to accelerate the reaction rate. As expected, the Ag/BOC samples exhibit outstanding photocatalytic activity, The photocatalytic activity increases form 40% to 54% with increasing Ag content from 1.0 to 5.0%, much higher than that of $(BiO)_2CO_3$ microspheres, C-doepd TiO_2 (25%),[42] N-doped TiO_2 (36%),[42] C_3N_4 (33%)[43] and BiOBr (21%).[44] Further increasing the Ag loading could result in a decrease in photocatalytic activity. A drastic decrease in photocatalytic activity is observed in Ag/BOC-20%, which can be ascribed to the serious aggregation of Ag nanoparticles and un-uniform morphology of $(BiO)_2CO_3$ microspheres (Fig. S3a). The aggregated Ag nanoparticles are not favorable for SPR effect and the un-uniform morphology of $(BiO)_2CO_3$ is not beneficial for SSR effect, which in all resulted in the decreased activity of Ag/BOC-20%.

The reaction intermediate of NO_2 during photocatalytic oxidation of NO is monitored on-line in the outlet as shown in Fig. 10b. The fraction of NO_2 generated over pure $(BiO)_2CO_3$ is relatively high during reaction. By Ag decoration, the fraction of NO_2 over the samples is decreased significantly, especially for the samples with low content of Ag. When the loading content of Ag is increased from 5% to 20%, the fraction of NO_2 is markedly increased because of the Ag particles aggregation and the destroying of the microspheres (Fig. S3b). However, the high fraction of NO_2 over Ag/BOC-20% is still lower than that of pure $(BiO)_2CO_3$. This fact implies that Ag decoration could promote the oxidation of intermediate NO_2 to final NO_3^- as shown in the following reactions.[25,34] The final oxidation products (nitric acid or nitrate ions) can be simply washed away by water wash.

$$NO + 2{\bullet}OH \rightarrow NO_2 + H_2O \quad (1)$$

$$NO_2 + {\bullet}OH \rightarrow NO_3^- + H^+ \quad (2)$$

$$NO + NO_2 + H_2O \rightarrow 2\ HNO_2 \quad (3)$$
$$NO + \bullet O_2^- \rightarrow NO_3^- \quad (4)$$

Considering the enhanced activity and inhibited NO_2 generation, the 5% Ag content is an optimum to achieve the highest photocatalytic performance. The above results indicate that appropriate amount of Ag loading could play a pivotal role in enhancing the visible light photocatalytic performance of $(BiO)_2CO_3$ microspheres.

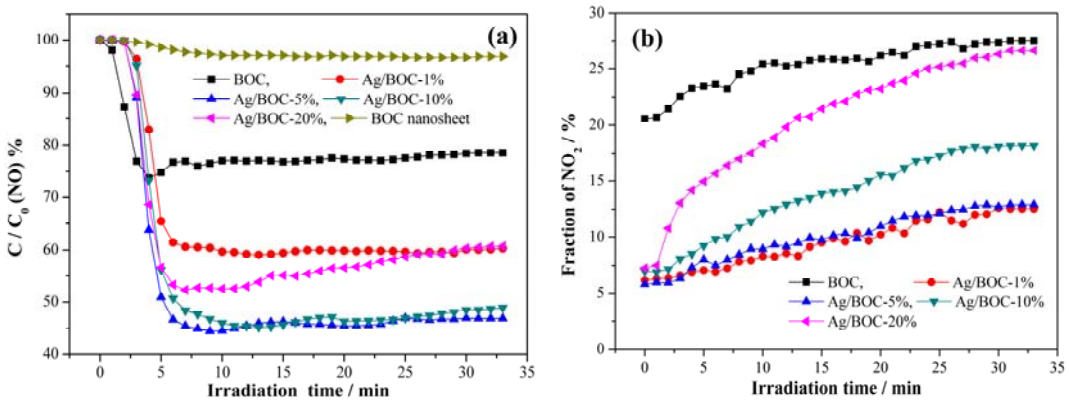

Fig. 10 Visible light photocatalytic activity of Ag-decorated $(BiO)_2CO_3$ and pure $(BiO)_2CO_3$ samples for the removal of NO in air (a). And the monitoring of the fraction of NO_2 intermediate over the samples during photocatalytic reaction. (Continuous reactor, NO concentration: 600 ppb).

Photocurrent generation was carried out for BOC nanosheet, BOC microsphere and Ag-BOC-5% electrodes to evaluate the electronic interaction between Ag and $(BiO)_2CO_3$ microspheres shown in Fig. 11a. It can be seen that steady and prompt photocurrent generation is obtained during on and off cycles of visible light illumination. The BOC nanosheets sample shows almost no photocurrent responses due to its large band gap. The BOC microspheres show decent photocurrent under visible light due the SSR effects, consistent with its photocatalytic activity. The charge transport in this as-prepared sample proceeds quickly, making the changes of "on" and "off" currents are nearly vertical. It is significant to observe that the photocurrent of the Ag-BOC-5% electrode is higher than that of the pure BOC microsphere electrode shown in Fig. 11a. The photocurrent enhancement of Ag-BOC can be ascribed to the enhanced photo-generated electrons/holes separation and the increased visible light adsorption of plasmonic Ag nanosrystal .[45,46]

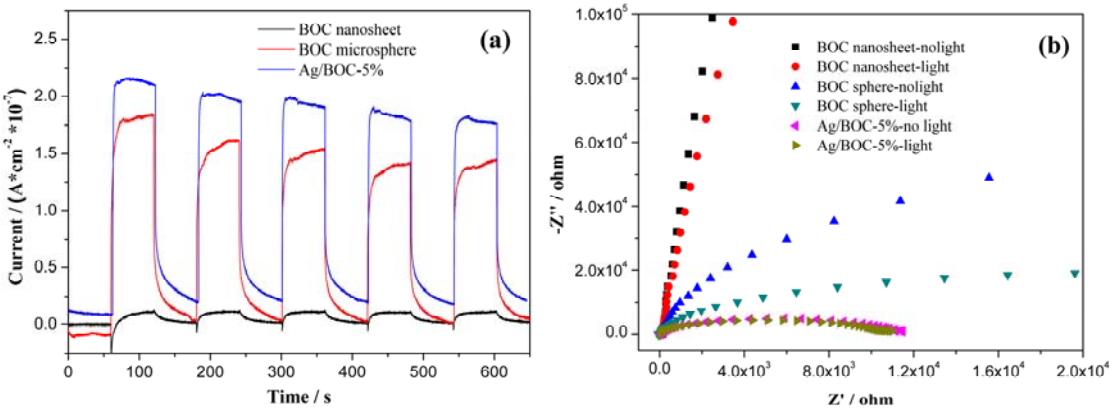

Fig. 11 Photocurrent generation (a) and Nyquist plots for BOC nanosheet, BOC microsphere and Ag-BOC-5% electrodes under visible light irradiation (λ> 420 nm, $[Na_2SO_4]$ = 0.5 M).

The separation efficiency of photo-generated electrons/holes pairs is a key factor for enhancement of photocatalytic activity and photocurrent. The interface charge separation efficiency was investigated by EIS shown in Fig. 11b. Fig. 11b showed the EIS Nyquist plots of BOC nanosheet, BOC microsphere and Ag-BOC-5% electrodes without and with irradiation. The radius of the arc on the EIS spectra indicates the reaction rate occurring at the surface of the electrode.[45,46] The smaller arc radius on the EIS Nyquist plot of Ag-BOC-5% under visible light irradiation implies that a more efficient separation of photo-generated electron/hole pairs and a faster interfacial charge transfer occurred in the interface of Ag nanosrystals and $(BiO)_2CO_3$ microspheres. It was also noted that the arc radius on the EIS Nyquist plot of Ag-BOC-5% was smaller than that of pure $(BiO)_2CO_3$ microspheres without irradiation. This fact suggests that the surface decoration of

Ag nanocrystals could change the distribution of charge carriers on $(BiO)_2CO_3$ microspheres and make the charge transfer easier.[45,46] These results imply that the coupling of Ag nanosrystals with $(BiO)_2CO_3$ microspheres can effectively improve the separation efficiency of photo-generated electron/hole pairs, consistent with the results from PL (Fig. 8) and time-resolved fluorescence spectra (Fig. 9).

3.7 Mechanism of activity enhancement by plasmonic Ag decoration

As previous studies shown that the enhancement in photocatalytic performance can be ascribed to the synergetic effects of many factors, such as hierarchical structure, surface area, interfacial charge transfer and efficient separation of photoinduced electrons and holes.[42,47-52] According to the above characterizations, the enhanced photocatalytic activity of Ag/BOC can be attributed to the congenerous effects of the following factors. Firstly, the SPR effect of spatially confined electrons in deposited Ag nanoparticles propels the Ag/BOC samples to absorb more visible light, which has been demonstrated by UV-vis DRS analysis. Also, owing to the SPR effect, the Ag nanoparticles can be photoexcited, thus enhancing the surface electron excitation and interfacial electron transfer.[53-55] Second, since the Fermi level of metal Ag (0.4 eV) is lower than the conduction band of $(BiO)_2CO_3$ (0.20 eV), the photogenerated electrons would probably transfer from $(BiO)_2CO_3$ to deposited Ag nanoparticles (as shown in Fig. 12),[56] creating a Schottky barrier at the interface that reduces the recombination of electron-hole pairs and increases the lifetime of charge carriers (Fig. 8 and 9). After the separation of electrons and holes, these two kinds of photogenerated charge carriers would be transformed into active species ($^{\cdot}OH$) that are responsible for the degradation of pollutants. As the redox potential of O_2/OH^- is 0.401 eV, the photoexcited electrons of Ag together with the electrons transferred from $(BiO)_2CO_3$ can reduce O_2 to OH^-. Meanwhile, the potential of the holes at the VB of $(BiO)_2CO_3$ (3.53 eV) is more positive than the redox potential of $OH^-/^{\cdot}OH$ (1.99 eV), and therefore the holes can oxidize OH^- to $^{\cdot}OH$. The OH^- radicals as major reactive oxidation species could oxidize the NO to final NO_3^- product.

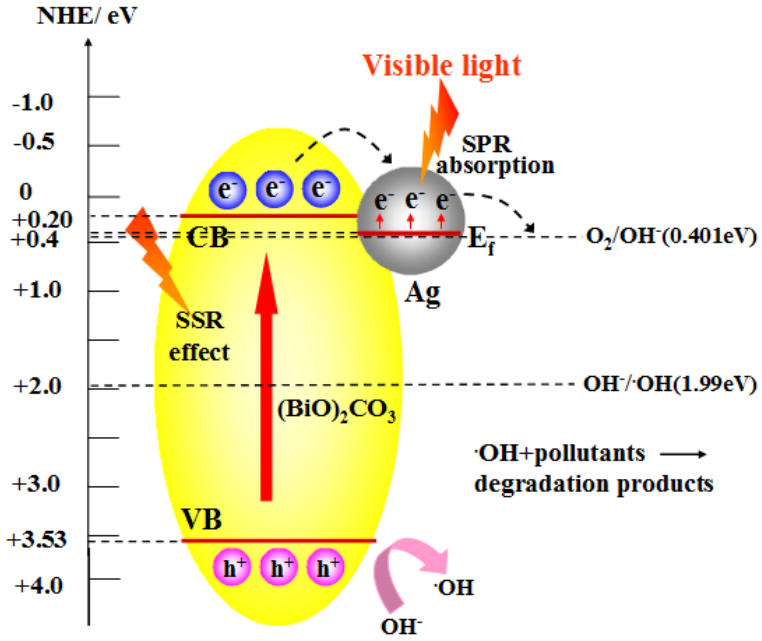

Fig. 12 photocatalytic mechanism scheme of Ag-decorated $(BiO)_2CO_3$ under visible light irradiation.

In order to put the as-prepared samples into practical applications, the photocatalytic stability of the samples was tested. An ideal photocatalyst should maintain photochemical stability and durability under long time irradiation so that it can be used repeatedly.[34] Fig. 13 shows the long term photocatalytic activity of Ag/BOC-5% under visible light irradiation. It's significant to find that the photocatalytic efficiency of Ag/BOC-5% does not exhibit obvious loss after five recycles, indicating that the Ag/BOC is relatively stable and not photo-corroded during the photocatalytic process. The photochemical stability of Ag/BOC can probably ascribed to the fact that reactants and products can transfer fast in the special hierarchical structures of $(BiO)_2CO_3$ microspheres instead of accumulating on the surface, thus effectively preventing the photocatalyst form deactivating.

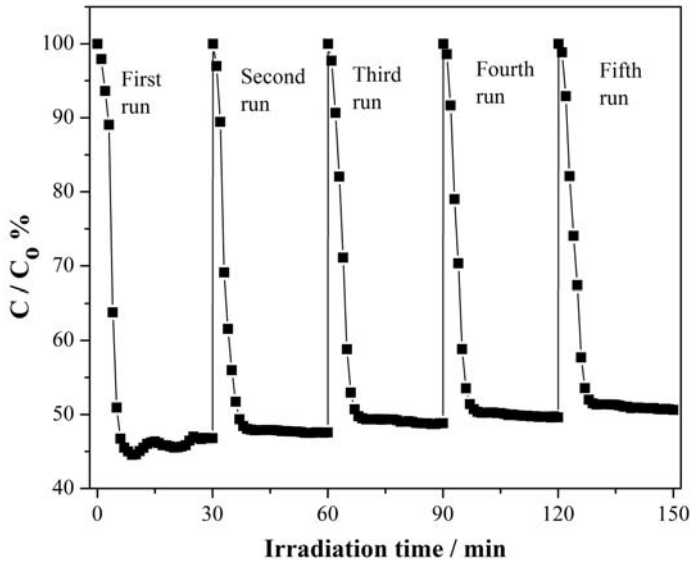

Fig. 13 Repeated visible light photocatalytic runs of Ag/BOC-5% for the removal of NO in air.

4. Conclusion

In summary, novel 0D Ag nanocrystals decorated 3D $(BiO)_2CO_3$ hierarchical microspheres were fabricated by a one-pot hydrothermal method for the first time. In the hydrothermal process, Ag^+ was in situ reduced to metal Ag nanocrystals by citrate ions and then deposited on the surface of $(BiO)_2CO_3$ microspheres. The pure $(BiO)_2CO_3$ microspheres exhibited decent visible light photocatalytic performance because of the multiple light reflecting and scattering effects induced by the special 3D hierarchical architectures. The Ag/BOC samples exhibited drastically enhanced visible light photocatalytic activity and promoted NO_2 oxidation towards NO removal than $(BiO)_2CO_3$ microspheres, which can be ascribed to the cooperative contribution of SSP effect, SPR effect, efficient separation of electron-hole pairs and prolonged lifetime of charge carriers by Ag nanoparticles. Among the as-prepared samples, Ag/BOC-5% with well-maintained morphology showed the highest photocatalytic activity, which suggested that the amount of Ag loading play a key role in enhancing the visible light photocatalytic activity of $(BiO)_2CO_3$ microspheres. Further increasing the Ag loading content could promote the aggregation of Ag particles and transform the $(BiO)_2CO_3$ into un-uniform microspheres. In addition, the as-prepared Ag/BOC-5% sample exhibited high photochemical stability and durability. The present results demonstrate that combing the SSR and SPR effects could make the Ag/BOC composite become a powerful and durable visible light driven photocatalyst for environmental pollution control. The present work could provide new insights into the in situ fabrication of noble metal/bismuth-based plasmonic photocatalysts with novel nano/micro structures.

Acknowledgements

This research is financially supported by the National Natural Science Foundation of China (51108487, 51102245), the Natural Science Foundation of Chongqing (cstc2013jcyjA20018), and the Innovative Research Team Development Program in University of Chongqing (KJTD201314).

Reference

[1] Y. Halpin, M. T. Pryce, S. Rau, D. Dini and J. G. Vos, *Dalton Trans.*, 2013, **42**, 16243-16254.
[2] H. F. Cheng, B. B. Huang and Y. Dai, *Nanoscale*, 2014, **6**, 2009-2026.
[3] J. H. Sun, J. S. Zhang, M. W. Zhang, M. Antonietti, X. Z. Fu and X. C. Wang, *Nat. Commun.*, 2012, **3**, 1139.
[4] L. G. Devi and R. Kavitha, Appl. Catal. B, 2013, 140-141, 559-587.
[5] C. W. Dunnill and I. P. Parkin, *Dalton Trans.*, 2011, **40**, 1635-1640
[6] S. Sarina, E. R. Waclawlk and H. Y. Zhu, *Green. Chem.*, 2013, **15**, 1814-1833.
[7] S. Linic, P. Christopher and D. B. Ingram, *Nature. Mater.*, 2011, **10**, 911-921.
[8] S. K. Cushing, J. T. Li, F. Meng, T. R. Senty, S. Suri, M. J. Zhi, M. Li, A. D. Bristow and N. Q. Wu, *J. Am. Chem. Soc.*, 2012, **134**, 15033-15041.
[9] P. Wang, B. B. Huang, Y. Dai and M. H. Whangbo, *Phys. Chem. Chem. Phys.*, 2012, **14**, 9813-9825.

[10] P. Wang, B. B. Huang, X. Y. Qin, X. Y. Zhang, Y. Dai, J. Y. Wei and M. H. Whangbo, *Angew. Chem. Int. Ed.*, 2008, **47**, 7931-7933.

[11] P. Wang, B. B. Huang, X. Y. Zhang, X. Y. Qin, H. Jin, Y. Dai, Z. Y. Wang, J. Y. Wei, J. Zhan, S. Y. Wang, J. P.Wang and M. H. Whangbo, *Chem. Eur. J.*, 2009, **15**, 1821-1824.

[12] Z. K. Zheng, B. B. Huang, X. Y. Qin, X. Y. Zhang, Y. Dai and M. H. Whangbo, *J. Mater. Chem.*, 2011, **21**, 9079-9087.

[13] R. H. Li, W. X. Chen, H. Kobayashi and C. X. Ma, *Green Chem.*, 2010, **12**, 212-215.

[14] J. G. Yu, G. P. Dai and B. B. Huang, *J. Phys. Chem. C*, 2009, **113**, 16394-16401.

[15] J. F. Guo, B. W. Ma, A. Y. Yin, K. N. Fan and W. L. Dai, *Appl. Catal. B*, 2011, 101, 580-586.

[16] R. Chen, M. H. So, J. Yang, F. Deng and H. Z. Sun, *Chem. Commun.*, 2006, 2265-2267.

[17] G. Cheng, H. M. Yang, K. F. Rong, Z. Lu, X. L. Yu and R. Chen, *J. Solid. State. Chem.*, 2010, **183**, 1878-1883.

[18] Y. Zheng, F. Duan, M. Q. Chen and Y. Xie, *J. Mol. Catal. A*, 2010, **317**, 34-40.

[19] Y. Y. Liu, Z. Y. Wang, B. B. Huang, K. S. Yang, X. Y. Zhang, X. Y. Qin and Y. Dai, *Appl. Surf. Sci.*, 2010, **257**, 172-175.

[20] X. F. Cao, L. Zhang, X. T. Chen and Z. L. Xue, *CrystEngComm.*, 2011, **13**, 1939-1945.

[21] X. Zhang, Y. Zheng, D. G. McCulloch, L. Y. Yeo, J. R. Friend and D. R. MacFarlane, *J. Mater. Chem. A*, 2014, **2**, 2275-2282.

[22] P. Madhusudan, J. R. Ran, J. Zhang, J. G. Yu and G. Liu, *Appl. Catal. B*, 2011, **110**, 286-295.

[23] P. Madhusudan, J. G. Yu, W. G. Wang, B. Cheng and G. Liu, *Dalton. Trans.*, 2012, **41**, 14345-14353.

[24] F. Dong, W. K. Ho, S. C. Lee, Z. B. Wu, M. Fu, S. C. Zou and Y. Huang, *J. Mater. Chem.*, 2011, **21**, 12428-12436.

[25] F. Dong, S. C. Lee, Z. B. Wu, Y. Huang, M. Fu, W. K. Ho, S. C. Zou and B. Wang, *J. Hazard. Mater.*, 2011, **195**, 346-354.

[26] F. Dong, H. T. Liu, W. K. Ho, M. Fu and Z. B. Wu, *Chem. Eng. J.*, 2013, **214**, 198-207.

[27] S. J. Peng, L. L. Li, H. T. Tan, Y. Z. Wu, R. Cai, H. Yu, X. Huang, P. N. Zhu, S. Ramakrishna, M. Srinivasan and Q. Y. Yan, *J. Mater. Chem. A*, 2013, **1**, 7630-7638.

[28] C. Z. Wu and Y. Xie, *Chem. Commun.*, 2009, 5943-5957.

[29] H. Q. Jiang, M. Nagai and K. Kobayashi, *J. Alloys Compd.*, 2009, **479**, 821-827.

[30] H. Xu, H. M. Li, C. D. Wu, J. Y. Chu, Y. S. Yan, H. M. Shu and Z. Gu, *J. Hazard. Mater.*, 2008, **153**, 877-884.

[31] J. G. Yu and B. Wang, *Appl. Catal. B*, 2010, **94**, 295-302.

[32] J. G. Yu, Y. R. Su and B. Cheng, *Adv. Funct. Mater.*, 2007, **17**, 1984-1990.

[33] J. G. Yu, J. Zhang and S. W. Liu, *J. Phys. Chem. C*, 2010, **114**, 13642-13649.

[34] Z. H. Ai, W. K. Ho, S. C. Lee and L. Z. Zhang, *Environ. Sci. Technol.*, 2009, **43**, 4143-4150.

[35] H. F. Cheng, B. B. Huang, P. Wang, Z. Y. Wang, Z. Z. Lou, J. P. Wang, X. Y. Qin, X. Y. Zhang and Y. Dai, *Chem. Commun.*, 2011, **47**, 7054-7056.

[36] A. P. Zhang and J. Z. Zhang, *Appl. Surf. Sci.*, 2010, **256**, 3224-3227.

[37] H. Y. Li, W. B. Lu, J. Q. Tian, Y. L. Luo, A. M. Asiri, A. O. Al-Youbi and X. P. Sun, *Chem. Eur. J.*, 2012, **18**, 8508-8514.

[38] M. Rycenga, C. M. Cobley, J. Zeng, W. Y. Li, C. H. Moran, Q. Zhang, D. Qin and Y. N. Xia, *Chem. Rev.*, 2011, **111**, 3669-3712.

[39] B. Kraeutler and A. J. Bard, *J. Am. Chem. Soc.*, 1978, **100**, 5985-5992.

[40] J. Lee and W. Choi, *J. Phys. Chem. B*, 2005, **109**, 7399-7406.

[41] J. Y. Xiong, Z. B. Jiao, G. X. Lu, W. Ren, J. H. Ye and Y. P. Bi, *Chem. Eur. J.*, 2013, **19**, 9472-9475.

[42] Q. Y. Li, H. T. Liu, F. Dong and M. Fu, *J. Colloid. Interf. Sci.*, 2013, **408**, 33-42.

[43] F. Dong, M. Y. Ou, Y. K. Jiang, S. Guo and Z. B. Wu, *Eng. Chem. Res.*, 2014, **53**, 2318-2330.

[44] W. D. Zhang, Q. Zhang and F. Dong, *Eng. Chem. Res.*, 2013, **52**, 6740-6746.

[45] Y. Zhou; Q. Zhang,; Y. H. Li, E. Antonova, W. Bensch and G. R. Patzke, *Sci. China Chem.*, 2013, **56**, 435-442.

[46] Y. J. Wang, X. J. Bai, C. S. Pan, J. He and Y. F. Zhu, *J. Mater. Chem.*, 2012, **22**, 11568-11573.

[47] Q. J. Xiang, J. G. Yu and M. Jaroniec, *Chem. Soc. Rev.*, 2012, **41**, 782-796.

[48] Q. Li, B. D. Guo, J. G. Yu, J. R. Ran, B. H. Zhang, H. J. Yan and J. R. Gong, *J. Am. Chem. Soc.*, 2011, **133**, 10878-10884.

[49] F. Dong, A. M. Zheng, Y. J. Sun, M. Fu, B. Q. Jinag, W. K. Ho, S. C. Lee and Z. B. Wu, *CrystEngComm*, 2012, **14**, 3534-3544.

[50] F. Dong, Y. J. Sun, W. K. Ho and Z. B. Wu, *Dalton. Trans.*, 2012, **41**, 8270-8284.

[51] F. Dong, Y. J. Sun, M. Fu, Z. B. Wu and S. C. Lee, *J. Hazard. Mater.*, 2012, **219-220**, 26-34.

[52] F. Dong, T. Xiong, Z. W. Zhao, Y. J. Sun and M. Fu, *CrystEngComm*, 2013, **15**, 10522-10532.

[53] M. J. Kale, T. Avanesian and P. Christopher, *ACS Catal.*, 2014, **4**, 116-128.

[54] J. Ren, W. Z. Wang, S. M. Sun, L. Zhang and J. Chang, *Appl. Catal. B*, 2009, **92**, 50-55.

[55] D. J. Wang, G. L. Xue, Y. Z. Zhen, F. Fu and D. S. Li, *J. Mater. Chem.*, 2012, **22**, 4751-4758.

[56] S. J. Peng, P. N. Zhu, S. G. Mhaisalkar and S. Ramakrishna, *J. Phys. Chem. C*, 2012, **116**, 13849-13857.

[57]